Temperature dependence of Raman scattering in ZnO

Ramon Cuscó, Esther Alarcón-Lladó, Jordi Ibáñez, and Luis Artús
Institut Jaume Almera, Consell Superior d'Investigacions Científiques (CSIC), Lluís Solé i Sabarís s.n., 08028 Barcelona, Spain

Juan Jiménez
Dept. Física de la Materia Condensada, ETSII, Universidad de Valladolid, Spain

Buguo Wang
Solid State Scientific Corporation, 27-2 Wright Road, Hollis, New Hampshire 03049, USA

Michael J. Callahan
Air Force Research Laboratory, Sensors Directorate, Electromagnetics Technology Division, Optoelectronic Technology Branch, Hanscom AFB, Massachusetts 01731-2909, USA

(Received 22 November 2006; published 6 April 2007)

We present a Raman scattering study of wurtzite ZnO over a temperature range from 80 to 750 K. Second-order Raman features are interpreted in the light of recent *ab initio* phonon density of states calculations. The temperature dependence of the Raman intensities allows the assignment of difference modes to be made unambiguously. Some weak, sharp Raman peaks are detected whose temperature dependence suggests they may be due to impurity modes. High-resolution spectra of the E_2^{high}, $A_1(\text{LO})$, and $E_1(\text{LO})$ modes were recorded, and an analysis of the anharmonicity and lifetimes of these phonons is carried out. The E_2^{high} mode displays a visibly asymmetric line shape. This can be attributed to anharmonic interaction with transverse and longitudinal acoustic phonon combinations in the vicinity of the K point, where the two-phonon density of states displays a sharp edge around the E_2^{high} frequency. The temperature dependence of the linewidth and frequency of the E_2^{high} mode is well described by a perturbation-theory renormalization of the harmonic E_2^{high} frequency resulting from the interaction with the acoustic two-phonon density of states. In contrast, the $A_1(\text{LO})$ and $E_1(\text{LO})$ frequencies lie in a region of nearly flat two-phonon density of states, and they exhibit a nearly symmetric Lorentzian line shape with a temperature dependence that is well accounted for by a dominating asymmetric decay channel.

DOI: 10.1103/PhysRevB.75.165202 PACS number(s): 78.30.Fs, 78.30.−j, 63.20.−e

I. INTRODUCTION

The interest in ZnO has been renewed by its potential applications in transparent electronics and UV optoelectronic devices. Its large exciton binding energy (60 meV) makes it highly attractive for applications as blue and ultraviolet light emitters, where it may become an advantageous alternative to GaN.[1] Good knowledge of the vibrational properties of this material is essential to understand transport properties and phonon interaction with the free carriers, both of which have great impact on optoelectronic device performance. Today this is made possible by the availability of high-quality, large-area bulk ZnO single crystals. In polar semiconductors, carriers excited high in the conduction band relax toward their ground state mainly by Fröhlich interaction with the longitudinal optical phonons. Thus, the dynamics of the phonon population strongly affects the performance of high-speed optoelectronic devices.[2] Raman scattering measurements are well suited to obtain information about the sample quality in wide band gap semiconductors[3–5] as well as to analyze more specific aspects of lattice dynamics, such as isotopic effects[6,7] and phonon lifetimes.[8,9] The temperature dependence of the phonon modes has also been used to determine the local temperature of a GaN diode as a function of the operating voltage,[10] and therefore Raman scattering has proven to be well suited to monitor the local temperature during device operation.

Wurtzite-type ZnO belongs to the space group C_{6v}^4 with two formula units in the primitive cell. The zone-center optical phonons can be classified according to the following irreducible representations: $\Gamma_{\text{opt}}=A_1+E_1+2E_2+2B_1$. The B_1 modes are silent modes, the A_1 and E_1 modes are polar modes and are both Raman and infrared active, whereas the E_2 modes are nonpolar and Raman active only. Polarized right-angle Raman scattering of ZnO was measured by Damen *et al.*[11] back in 1965. Arguello *et al.*[12] reported Raman spectra of ZnO obtained in a variety of geometries, which allowed them to identify all Raman active modes from their selection rules. A few years later, a detailed study of the resonant behavior of the high frequency E_2 mode (E_2^{high}), $A_1(\text{TO})$, and $E_1(\text{TO},\text{LO})$ modes as well as several second-order features was presented by Calleja and Cardona.[13] Data on temperature dependence of ZnO phonons also date back to the late 1970s.[14] In the past few years, the availability of bulk ZnO crystals of very high optical quality and the technological relevance of this material have spurred the realization of fundamental and more detailed studies on ZnO lattice dynamics. However, our knowledge of the lattice dynamics of ZnO is still rather limited, as few experimental data are available on phonon dispersion in this material. In fact, detailed measurements of the optical phonon branch by inelastic neutron scattering are still lacking. Only recently have *ab initio* density-functional theory (DFT) calculations of lattice-dynamical properties been published,[15] which have made a

TABLE I. Symmetry allowed Raman modes for the scattering geometries considered in this work.

	Raman active modes				
Scattering geometry	E_2	A_1(LO)	A_1(TO)	E_1(LO)	E_1(TO)
$z(xx)\bar{z}$	A	A			
$z(xy)\bar{z}$	A				
$x(yy)\bar{x}$	A		A		
$x(zy)\bar{x}$					A
$x(zy)y$				A	A

more accurate interpretation of the experimental data possible. Thus, the unusual variations of the E_2^{high} phonon linewidth with the isotopic composition and with pressure have been accounted for by fine features of the phonon density of states (DOS) revealed by the DFT calculations.[8] Recently, the low-frequency E_2 phonon lifetime has been measured in ZnO by means of impulsive stimulated Raman scattering experiments, and it has been found to be longer than 200 ps at low temperature.[16] It has been suggested that such long-lived optical phonons could have applications in quantum cryptography and quantum computing.[16]

In this work we present a study of the first- and second-order Raman spectra of ZnO and their dependence on temperature. Second-order Raman features are discussed in the light of recently available DFT calculations of phonon DOS. To analyze the temperature dependence of optical phonons in ZnO, high spectral resolution measurements of the E_2^{high}, A_1(LO), and E_1(LO) modes have been carried out at different temperatures. A visible line-shape asymmetry is observed for the E_2^{high} mode, which can be explained by the features of the two-phonon DOS around the E_2^{high} frequency. We discuss the temperature effects on the phonons in terms of third-order anharmonic decay. Whereas the behavior of the A_1(LO) and E_1(LO) modes is well described by a dominant decay channel localized around a single set of frequencies, the description of the E_2^{high} temperature dependence requires a more detailed analysis that takes into account the two-phonon DOS.

II. EXPERIMENT

The experiments were performed on a high-quality ZnO single crystal obtained by the hydrothermal growth method. Growth details as well as x-ray and photoluminescence (PL) characterization of ZnO crystals obtained by this method have been published elsewhere.[17] After chemomechanical polish, PL spectra obtained at 2.1 K revealed emission from excitonic transitions with narrow line shapes, indicating the high quality of these hydrothermally grown samples.[17]

The Raman spectra were excited with the 514.5 nm line of an Ar^+ laser in different scattering geometries (see Table I). The scattered light was analyzed by means of a Jobin-Yvon T64000 triple spectrometer equipped with a LN_2-cooled charge-coupled device (CCD) detector. Full-range spectra were obtained in the subtractive configuration of the spectrometer with 100 μm slits, corresponding to a spectral slit width of $\approx$2.5 cm^{-1}. The triple additive configuration with 50 μm slit was utilized to obtain high resolution spectra of the E_2^{high}, A_1(LO), and E_1(LO) modes. The spectrometer spectral broadening for this configuration was checked by measuring the λ=546.07 nm emission line of Hg, which was fitted by a Gaussian line shape with a full width at half maximum (FWHM) of Γ_G=0.44 cm^{-1}. Then, following Ref. 8, the instrumental broadening was estimated from $\Gamma_L=\Gamma-\Gamma_G^2/\Gamma$, where Γ and Γ_L are, respectively, the FWHM measured on the Raman spectrum and the intrinsic FWHM of the mode. Using this relation, we find that the instrumental broadening correction for the narrowest mode studied (the E_2^{high} mode at 80 K) amounts to less than 1% of the measured FWHM, and therefore we can assume that the high-resolution Raman spectra reflect the intrinsic FWHM of the modes.

A LN_2 cryostat was used to vary the sample temperature from 80 to 380 K. Within this temperature range, the spectra were acquired in macrocamera configuration. To extend the temperature range up to 750 K, we used a Linkam high-temperature stage and the measurements were performed using a confocal microscope with a long working-distance $\times$80 objective protected by a cooling jacket. Both sets of measurements yield consistent results in the overlapping temperature range between 290 and 380 K. For each measurement, the temperature was stabilized for 10 min before acquiring a spectrum.

III. RESULTS AND DISCUSSION

A. First- and second-order Raman scattering of ZnO

First, we present an overview of the first-order Raman scattering in ZnO, and compare our results with previously reported data. We have performed polarized Raman scattering measurements in different scattering configurations to identify all Raman active modes of ZnO (see Table I). The Raman tensors for each of these modes are given by

$$E_2^{(1)}=\begin{pmatrix} d & 0 & 0 \\ 0 & -d & 0 \\ 0 & 0 & 0 \end{pmatrix}, \quad E_2^{(2)}=\begin{pmatrix} 0 & d & 0 \\ d & 0 & 0 \\ 0 & 0 & 0 \end{pmatrix},$$

$$E_1(x)=\begin{pmatrix} 0 & 0 & c \\ 0 & 0 & 0 \\ c & 0 & 0 \end{pmatrix}, \quad E_1(y)=\begin{pmatrix} 0 & 0 & 0 \\ 0 & 0 & c \\ 0 & c & 0 \end{pmatrix},$$

$$A_1(z)=\begin{pmatrix} a & 0 & 0 \\ 0 & a & 0 \\ 0 & 0 & b \end{pmatrix}. \tag{1}$$

For polar modes, the coordinate in parentheses denotes the direction of phonon polarization. As derived from the Raman tensors of the respective modes, all Raman active modes can be observed in backscattering geometry except for the E_1(LO) mode, for which only the polarizability components involving z and the direction of phonon polarization

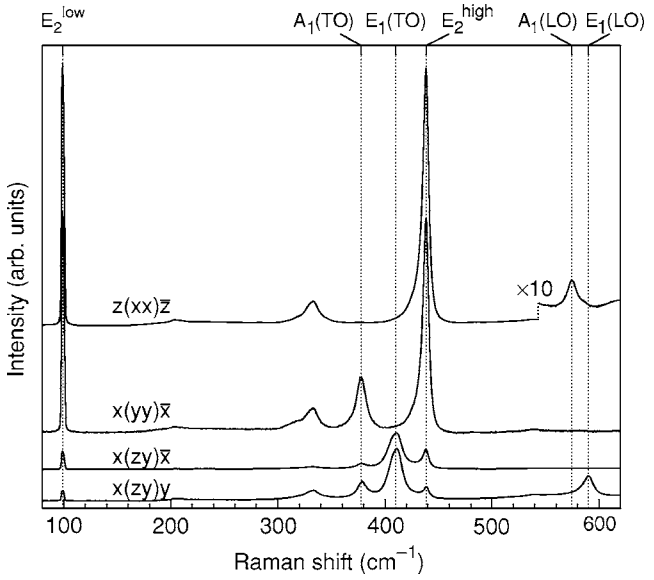

FIG. 1. Room temperature first-order Raman spectra of ZnO in scattering geometries corresponding to A_1+E_2 and E_1 symmetries.

change during the vibration. The symmetry-allowed Raman modes for the scattering geometries considered in this work are summarized in Table I for convenience. Although the E_1(LO) mode was reported in the forbidden configuration $x(zz)\bar{x}$ under 406.7-nm excitation owing to intraband Fröhlich interaction,[13] the unambiguous observation of the E_1(LO) mode requires a scattering configuration with a nonvanishing $x(zy)y$ component.

Figure 1 shows polarized first-order Raman spectra of the ZnO sample obtained at room temperature in four different scattering configurations that allow the observation of all the Raman active modes. Our results are consistent with previous Raman studies.[11–13] The $z(xx)\bar{z}$ spectrum (E_2+A_1 symmetry) is dominated by the two intense, sharp E_2 modes at 99 and 438 cm^{-1}. The low-frequency E_2 mode, involving mainly Zn motion, displays an extremely narrow linewidth, well below the slit width of the subtractive configuration of the spectrometer even for the highest temperature studied. The E_2^{high} mode displays a clear asymmetry toward low frequencies that we shall discuss in more detail in the next section. In contrast with previous works, where the A_1(LO) mode could not be detected for excitation wavelengths longer than 406.7 nm,[13] we can detect a weak A_1(LO) mode at 574 cm^{-1}. The prominent feature at 333 cm^{-1} corresponds to second-order scattering and will be discussed below. In the $x(yy)\bar{x}$ spectrum (E_2+A_1 symmetry), in addition to the strong E_2 modes a new peak appears at 378 cm^{-1}, which can be assigned to the A_1(TO) mode. An additional peak emerges at 410 cm^{-1} in the $x(zy)\bar{x}$ spectrum (E_1 symmetry), which is assigned to the E_1(TO) mode. Finally, the E_1(LO) mode can be observed at 590 cm^{-1} in the $x(zy)y$ spectrum. Therefore, the highest-frequency first-order mode of ZnO corresponds to the E_1(LO) mode, which at zone center is found at a frequency 16 cm^{-1} higher than that of the A_1(LO) mode. It is worth noting that DFT calculations yield inaccurate results regarding the E_1(LO) and A_1(LO) modes, as they give a zone center E_1(LO) frequency 4 cm^{-1} lower than that of the A_1(LO) mode.[15] This fact should be taken into account when discussing the Raman features of ZnO in terms of the calculated phonon DOS. The observed first-order Raman frequencies are reported in Table II.

A residual intensity of the forbidden E_2 modes can be seen in the $x(zy)\bar{x}$ and $x(zy)y$ spectra that could arise from a slight misalignment of the sample introducing a small x component in the z polarization direction or from a lower quality of the sample polishing in the m prismatic face resulting in a relaxation of the selection rules.

Whereas wave-vector conservation restricts the phonons involved in first-order Raman scattering to those with $\mathbf{k}\approx 0$, phonons from the entire Brillouin zone take part in second-order Raman scattering. Therefore, second-order spectra usually display feature-rich structures, which are determined, on the one hand, by the phonon DOS and, on the other hand, by the selection rules of the two-phonon scattering processes. Selection rules for two-phonon Raman scattering in crystals with the wurtzite structure were reported by Siegle *et al.*[18] As a general rule, it was found that overtones always contain the representation A_1 whereas combinations of phonons belonging to different representations do not contain the A_1 representation. According to DFT calculations[15] the phonon DOS of ZnO presents a frequency gap between acoustic and optical modes that extends from 270 to 410 cm^{-1}. The second-order spectra may then be divided into three regions: (i) the low-frequency region (approximately 160–540 cm^{-1}) dominated by acoustic overtones, (ii) the high-frequency region (820–1120 cm^{-1}) formed by optical overtones and combinations, and (iii) the intermediate-frequency region (540–820 cm^{-1}) where optical and acoustic phonon combinations occur.

In the present analysis, we use the phonon dispersion calculated by DFT (Ref. 15) and the symmetry selection rules for two-phonon Raman scattering reported by Siegle *et al.*[18] to aid the identification of the second-order features of the ZnO Raman spectrum. Figure 2 shows the $z(xx)\bar{z}$ polarized second-order Raman spectra of ZnO (A_1+E_2 symmetry) for different temperatures in the 80–300 K range. The second-order features are labeled with their respective frequencies on the RT spectrum. The most prominent second-order features occur in the high-frequency region and correspond to LO overtones and combinations involving LO modes. The broad, intense peak at 1158 cm^{-1}, which is found between the doubled frequencies measured for the A_1(LO) and E_1(LO) modes, contains contributions of $2A_1$(LO) and $2E_1$(LO) modes at the Γ point of the Brillouin zone, and possibly also of 2LO scattering by mixed modes from the rather flat bands along the *A*-*L*-*M* line. The weaker peak at 1105 cm^{-1} can be attributed to 2LO at *H* and *K*. Note that the DFT calculations, in addition to giving the wrong ordering for the E_1(LO) and A_1(LO) modes, tend to underestimate the LO frequencies. Thus, the Raman peaks in this region occur at higher frequencies than predicted by DFT results. As mentioned above, all these overtones contain the A_1 representation, and furthermore, they occur in a region with high two-phonon DOS. Two weak shoulders can be observed in the RT spectrum at 1072 and 1044 cm^{-1}, which become more vis-

TABLE II. Room temperature frequencies and symmetries of the first- and second-order Raman spectra observed in ZnO and their assignments. Our results are compared with previous data in Ref. 13. Parentheses indicate symmetries that although being present in the spectra display a much lower intensity than the dominant one.

Frequency (cm^{-1})				
Our data	Ref. 13	Symmetry	Process	Brillouin zone points/lines
99	101	E_2	E_2^{low}	Γ
203	208	$A_1,(E_2)$	2TA; $2E_2^{low}$	$L,M,H;\Gamma$
284		A_1	$B_1^{high}-B_1^{low}$	Γ
333	332	$A_1,(E_2,E_1)$	$E_2^{high}-E_2^{low}$	Γ
378	380	A_1	A_1(TO)	Γ
410	408	E_1	E_1(TO)	Γ
438	437	E_2	E_2^{high}	Γ
483		A_1	2LA	*M-K*
536	541	A_1	$2B_1^{low}$; 2LA	$\Gamma;L,M,H$
574	574	A_1	A_1(LO)	Γ
590	584	E_1	E_1(LO)	Γ
618		A_1	TA+TO	H,M
657		E_1,E_2	TA+LO	L,H
666		A_1	TA+LO	M
700		A_1	LA+TO	M
723		A_1	LA+TO	*L-M*
745		A_1	LA+TO	*L-M*
773		A_1	LA+TO	M,K
812		A_1	LA+LO	L,M
980	990	A_1	2TO	*L-M-K-H*
1044		A_1	TO+LO	A,H
1072	1080	A_1	TO+LO	M,L
1105		A_1	2LO	H,K
1158	1160	A_1	$2A_1$(LO),$2E_1$(LO); 2LO	Γ;*A-L-M*

ible at low temperature. We assign the mode at 1072 cm^{-1} to TO+LO combinations at the *M* and *L* points, and the mode at 1044 cm^{-1} to TO+LO combinations at the *A* and *H* points. A weak broad band can be observed at about 980 cm^{-1}, which can be attributed to TO overtones. It is noteworthy that the scattering efficiency of processes involving LO modes is much higher than those involving TO modes. As reported by Calleja and Cardona,[13] the 2LO scattering is resonantly enhanced already at photon energies ~1 eV below the fundamental gap.

A multiplicity of structures appear in the low- and intermediate-frequency regions of the spectra, where acoustic overtones and acoustic-optical combinations occur. To aid their identification by analyzing their symmetry, we have recorded polarized Raman spectra in several scattering geometries. In Fig. 3 we display the A_1+E_2, A_1, E_2, and E_1 components of the second-order spectrum. The most intense peak in the intermediate-low-frequency region is observed at 333 cm^{-1}. This mode had been previously assigned to transverse acoustic overtone scattering at *M*.[13,19] However, the temperature dependence of its Raman intensity (see Fig. 2) clearly indicates that this is a difference mode. The frequency of this mode is in good agreement with the difference between the E_2^{high} and E_2^{low} frequencies measured in our sample. Using the notation of Ref. 18, the $E_2^{high}-E_2^{low}$ difference contains symmetries $\Gamma_6\otimes\Gamma_6\supset A_1,E_2$. This is consistent with the polarized measurements shown in Fig. 3, which indicate that the symmetry of the 333 cm^{-1} mode is predominantly A_1, with a smaller E_2 component and an even smaller E_1 component. According to the calculated phonon dispersion relations,[15] the 333-cm^{-1} mode could also contain contributions from $[\mathrm{TO}-\mathrm{TA}]_{A,L,H}$ differences. These differences, however, yield higher frequencies and all of them contain the E_1 symmetry. To demonstrate the origin of the 333-cm^{-1} mode, we plot in Fig. 4 the Raman intensity of this mode versus temperature, normalized to its intensity at room temperature, and we compare it with the statistical occupation factor for the $E_2^{high}-E_2^{low}$ difference mode (dashed line), which is given by[20]

$$\rho(T)=[1+n(E_2^{high})]n(E_2^{low}), \tag{2}$$

where $n(E)=[\exp(E/k_BT)-1]^{-1}$ is the Bose-Einstein distribution function. For comparison, we also plot (dotted line)

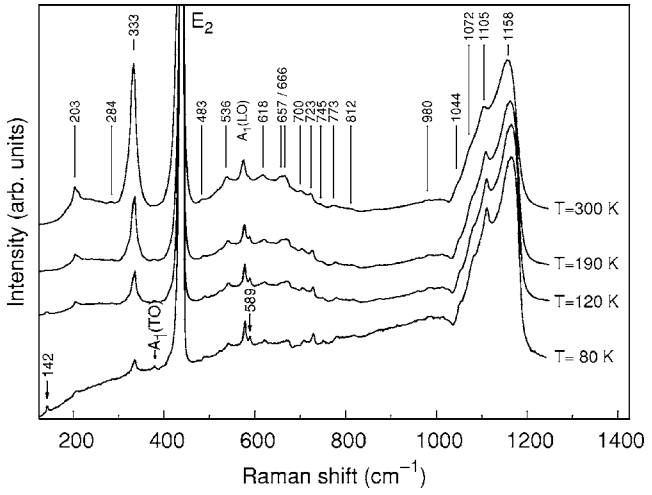

FIG. 2. Second-order Raman spectra of ZnO obtained in $z(xx)\bar{z}$ configuration for temperatures in the 80–300 K range.

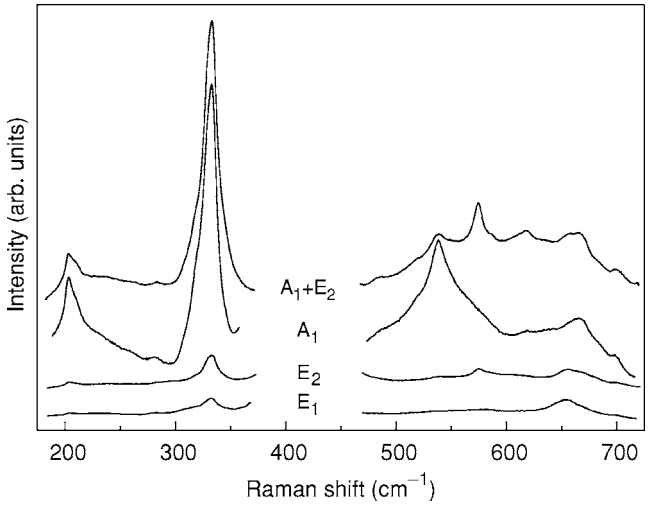

FIG. 3. Second-order Raman spectra of ZnO obtained for various scattering geometries. From top to bottom, $z(xx)\bar{z}$, $x(zz)\bar{x}$, $z(xy)\bar{z}$, and $x(zy)\bar{x}$.

the statistical occupation factor for overtones of TA phonons with $\hbar\omega_{\mathrm{TA}} \approx 160\ \mathrm{cm}^{-1}$ around the M point, $\rho(T)=[1+n(\hbar\omega_{\mathrm{TA}})]^2$, as suggested in Refs. 13 and 19. Clearly, the statistical occupation factor for the difference mode [Eq. (2)] accounts for the observed temperature dependence of the intensity, whereas the corresponding factor for the overtones deviates significantly from the experimental points.

Another prominent peak is observed at 203 cm^{-1}, which as seen from Fig. 3 exhibits A_1 symmetry and thus can be attributed to a TA overtone. In Ref. 15 this mode was assigned to $2\mathrm{TA}_L$, and in Ref. 13 to $2E_2^{\mathrm{low}}$ with possible contributions of 2TA at the M point. We note that the corresponding phonon branch is rather flat at H, so we speculate that the 203 cm^{-1} peak could also have a significant contribution of 2TA scattering at the H point.

A weak peak can be seen at 284 cm^{-1} in the room temperature spectrum, which disappears at lower temperatures (see Fig. 2), and therefore we assign it to a difference mode. As can be seen from Fig. 3, this mode has A_1 symmetry. Several mode differences yield frequencies close to the observed peak: $A_1(\mathrm{LO})-B_1^{\mathrm{low}}$, $E_1(\mathrm{LO})-B_1^{\mathrm{low}}$, $B_1^{\mathrm{high}}-B_1^{\mathrm{low}}$, and $[\mathrm{LO\text{-}LA}]_L$. However, some of them have symmetries which are incompatible with the spectra of Fig. 3. The symmetry of these differences are, respectively, $\Gamma_1\otimes\Gamma_3\supset B_1$, $\Gamma_5\otimes\Gamma_3\supset E_2$, $\Gamma_3\otimes\Gamma_3\supset A_1$, and $L_{\mathrm{I}}\otimes L_{\mathrm{I}}\supset A_1, E_1, E_2$.[18] Therefore, the first two possibilities can be excluded, and the absence of E_1 and E_2 component in this peak suggests that it can be primarily assigned to B_1^{high}-B_1^{low}. The very weak structure detected at 483 cm^{-1}, which as seen from Fig. 3 exhibits A_1 symmetry, can be assigned to LA overtones along M-K, where phonon dispersion is nearly flat and hence the DOS is very high. The peak at 536 cm^{-1} is clearly of A_1 symmetry and can be attributed to $2B_1^{\mathrm{low}}$ and LA overtones along L-M and H.

Above this frequency, we find acoustic and optical combinations. The peak at 618 cm^{-1} could be tentatively assigned to TA+TO at the H and M points. TA+LO combinations give rise to the doublet observed at 657–666 cm^{-1}. The lower component of the doublet has E_2 and E_1 symmetry, whereas the symmetry of the higher component is basically A_1. The highest DOS for combinations in this frequency range is found at the L, M, and H points. Both at the L and H points the TA+LO combination has symmetry E_1, E_2, whereas at the M point combinations of the type $M_i\otimes M_i\supset A_1, E_2$ occur. This suggests the assignment of the 657 cm^{-1} mode to TA+LO combinations at the L and H points and the 666 cm^{-1} mode to TA+LO combinations at the M point. Low intensity modes of mainly A_1 symmetry are detected at 700, 723, 745, 773, and 812 cm^{-1}, which can be attributed to acoustic and optical combinations. Taking into account the predominantly A_1 symmetry of all these modes, we tentatively assign the peak at 700 cm^{-1} to LA+TO combinations at the M point, and the peak at 812 cm^{-1} to LO+LA combinations at the L and M points. The frequencies of the second-order Raman features observed at room temperature are collected in Table II.

It is noteworthy that, in addition to the second-order peaks discussed above, several sharp peaks appear and grow in intensity as the temperature decreases. These peaks are

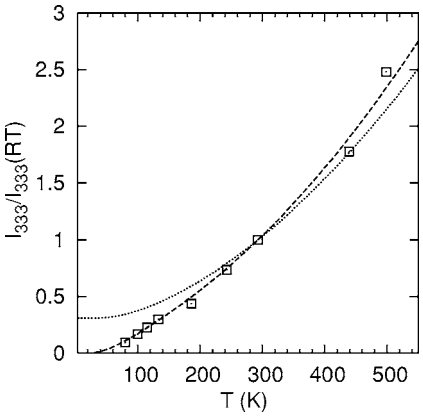

FIG. 4. Intensity of the second-order peak observed at $\approx$333 cm^{-1} as a function of temperature. Dashed line, occupation number factor for the $E_2^{\mathrm{high}}-E_2^{\mathrm{low}}$ difference mode; dotted line, *idem* for TA overtones around the M point.

marked by arrows in the 80 K spectrum shown in Fig. 2. The weak peak at 380 cm^{-1} appears at the same frequency as the $A_1(TO)$ mode in a $x(yy)\bar{x}$ spectrum recorded at 80 K, so we assign it to a leaky $A_1(TO)$ mode. While the peak at 589 cm^{-1} is close to the $E_1(LO)$ mode, its frequency is about 4 cm^{-1} lower than that measured for the $E_1(LO)$ mode at 80 K in the allowed $x(zy)y$ scattering configuration. This peak could be related to local vibrational modes associated with intrinsic lattice defects, similarly to the peak that was observed at 582 cm^{-1} in doped GaN,[3,19,21] which was conjectured to be associated with intrinsic lattice defects favored or activated by doping.[21] The intensity enhancement and sharpening with decreasing temperature observed for this peak as well as for that at 142 cm^{-1} clearly suggest a local mode origin for these peaks. Although Al, Fe, Si, Li, and K impurities were detected by glow discharge mass spectrometry in hydrothermal ZnO samples, their concentration was found to be in the few ppm range,[17] well below the detection limit of Raman spectroscopy. Thus, we speculate that these peaks are related to intrinsic lattice defects, which may be favored by the growth conditions. These crystals present a strong visible luminescence band, which supports the existence of intrinsic point defects. On the other hand, surface effects can be ruled out because of the deep penetration of the excitation light. Further work should be carried out to determine the origin of these Raman peaks.

B. Anharmonic phonon decay and phonon lifetimes

1. The E_2^{high} mode: Fermi resonance model

In the discussion of the first-order Raman spectra of ZnO presented in the preceding section, we noted that the E_2^{high} mode exhibits a visibly asymmetric line shape with a low-frequency tail. This is quite apparent from Fig. 1 when one compares the line shapes of the E_2^{high} and $A_1(TO)$ modes. Given that the $A_1(TO)$ line shape is fairly symmetric, the asymmetry of the E_2^{high} mode cannot be ascribed to lattice disorder. Furthermore, isotopic broadening is negligible for the E_2^{high} mode since it mainly involves O motion, and O is nearly isotopically pure. The line-shape broadening is then mostly determined by anharmonic phonon-phonon interactions. These can result in strongly distorted peaks when resonant interaction with a band of second-order combinations takes place (Fermi resonance), as is the case, for instance, for the GaP TO mode,[22,23] where the presence of van Hove-type singularities in the DOS of the TA+LA combination band gives rise to a highly asymmetric TO mode, which develops a side band at high pressure.[22] A similar situation occurs for the E_2^{high} mode of ZnO, as its frequency lies close to a ridge-like structure of the two-phonon DOS corresponding to TA+LA combinations in the vicinity of the K point.[8]

To evaluate this effect for the E_2^{high} phonon of ZnO we consider the phonon self-energy $\Sigma(\omega)=\Delta(\omega)-i\Upsilon(\omega)$, which expresses the renormalization of the *bare* harmonic frequency of the mode, ω_0, as a result of the interaction with other phonons. To the second order in perturbation theory, the cubic anharmonicity effect on the imaginary part of the self-energy is given by[24]

$$\Upsilon(\omega)=\frac{18\pi}{\hbar^2}\sum_{\mathbf{q}j_1j_2}|V_3(\mathbf{q}j_1,-\mathbf{q}j_2)|^2[(n_1+n_2+1)\delta(\omega_1+\omega_2-\omega)+(n_2-n_1)\delta(\omega_1-\omega_2-\omega)], \tag{3}$$

where $V_3(\mathbf{q}j_1,-\mathbf{q}j_2)$ is the third-order coefficient in the expansion of the lattice potential in normal coordinates and n_1 and n_2 are the Bose-Einstein occupation factors for the modes $\omega(\mathbf{q},j_1)$ and $\omega(-\mathbf{q},j_2)$, respectively ($\mathbf{q}$ is the phonon wave vector and j_i labels the phonon branch). Assuming slowly varying Bose-Einstein factors and V_3 coefficients in the small energy range considered, the imaginary part of the self-energy is proportional to the two-phonon DOS and can be written as

$$\Upsilon(\omega)=|V_3^+|^2(1+n_1+n_2)\rho^+(\omega)+|V_3^-|^2(n_2-n_1)\rho^-(\omega), \tag{4}$$

with $\rho^+(\omega)$ and $\rho^-(\omega)$ the two-phonon sum and difference DOS, and V_3^+ and V_3^- the effective third-order anharmonic constants for decay into phonon sums and phonon differences, respectively. Since real and imaginary parts of the phonon self-energy are related by a Kramers-Kronig transformation, the corresponding real part of the self-energy $\Delta(\omega)$ can be evaluated as

$$\Delta(\omega)=-\frac{2}{\pi}\mathcal{P}\int_0^\infty\frac{\omega'}{\omega'^2-\omega^2}\Upsilon(\omega')d\omega'. \tag{5}$$

This yields a frequency-dependent renormalization of the phonon energy, which has to be added to the constant shift in frequency due to the thermal expansion of the lattice Δ_0. This latter contribution can be written as[25]

$$\Delta_0=-\omega_0\gamma\int_0^T[\alpha_c(T')+2\alpha_a(T')]dT', \tag{6}$$

where α_c and α_a are the linear thermal expansion coefficients along directions parallel and perpendicular to the c axis, respectively, and γ is the Grüneisen parameter of the E_2^{high} mode, which we take as $\gamma=2.02$.[15] We have derived the thermal expansion coefficients for ZnO from the temperature dependence of the lattice parameters determined by x-ray diffraction by Iwanaga *et al.*[26] Although these data are only available for $T\geq 300$ K, we have extrapolated the results down to $T=200$ K. Below this temperature, thermal expansion usually falls rapidly and becomes negligible at $T\sim 50$ K,[27] and consequently the extrapolation of high-temperature values is not a good approximation. Thus, as a more accurate approximation for the thermal expansion coefficients for $T<200$ K we have used the calculated variation for ZnSe,[27] scaled to fit smoothly with the curve derived from experimental results for ZnO. For small self-energy corrections compared to the Raman frequency, the line shape of the Raman peak is

$$I(\omega)\propto\frac{\Upsilon(\omega)}{[\omega_0+\Delta_0+\Delta(\omega)-\omega]^2+\Upsilon(\omega)^2}. \tag{7}$$

If the frequency dependence of the phonon self-energy is neglected, the Raman line shape given by Eq. (7) reduces to

a Lorentzian function. In that case, the imaginary part of the phonon self-energy gives directly the half width of the corresponding line shape $\Upsilon = \frac{1}{2}\Gamma$. Note, however, that because of the frequency dependence of the self-energy, the line shape given by Eq. (7) may deviate substantially from a Lorentzian line shape and the comparison between the Raman linewidth and the theoretical lifetime requires a detailed analysis that involves a calculation of both the real and the imaginary part of the self-energy.[28] We use Eq. (7) with the frequency-dependent self-energy in order to simulate the Raman spectrum of the E_2^{high} mode and explain the observed asymmetric line shape.

To evaluate the imaginary part of the self-energy we have used the two-phonon sum DOS reported by Serrano *et al.*,[8] shifted by -10 cm^{-1} as explained in Ref. 15. Following the approach taken in Refs. 6 and 23, we smooth the calculated DOS in order to avoid spurious artifacts in the calculated line shapes. On the other hand, the two-phonon difference DOS is nearly flat around the E_2^{high} frequency, and can be approximated by a constant value $\rho^-(\omega) \approx 0.25$ states/cm^{-1}, as given in Ref. 8. According to the calculated phonon dispersion of ZnO, the most likely decay channels for the E_2^{high} mode are the decay into two acoustic modes at $\omega_1 \approx 190$ cm^{-1} and $\omega_2 \approx 250$ cm^{-1}, and into a difference between a longitudinal optical mode at $\omega_2 \approx 550$ cm^{-1} and an acoustic mode at $\omega_1 \approx 110$ cm^{-1}.[8] Using the corresponding Bose-Einstein occupation factors in Eq. (4), the line shape of the E_2^{high} mode can be calculated from Eqs. (4)–(7) with two adjustable parameters $|V_3^+|^2$ and $|V_3^-|^2$. We have taken $\omega_0 = 440$ cm^{-1} as given by the *ab initio* calculations reported in Ref. 15. A rigid shift of the two-phonon sum DOS has been included to take into account the thermal expansion effects. This has been obtained from Eq. (6) with the average Grüneisen parameters of the acoustic modes at $\omega_1 \approx 190$ cm^{-1} and $\omega_2 \approx 250$ cm^{-1}, which, based on the values reported in Ref. 15, we take as $\bar{\gamma} \approx 1.1$.

In Fig. 5 we plot the real and imaginary parts of the phonon self-energy and the theoretical line shape (solid line) for room temperature and $|V_3^+|^2 = 39$ cm^{-2} and $|V_3^-|^2 = 5.8$ cm^{-2}. We shall discuss the determination of the anharmonic coupling constants below. The calculated line shape has been upshifted by 2.3 cm^{-1} to bring it into agreement with the experimental spectrum. Such frequency shift is necessary because of the low *bare* harmonic frequency given by the *ab initio* calculations, which was estimated to be about 0.7% too low in Ref. 15. Very good agreement is obtained with the high-resolution Raman spectrum of the E_2^{high} mode (open circles). As can be seen from Fig. 5, the E_2^{high} line shape exhibits an asymmetric broadening toward low frequencies, where it deviates significantly from the Lorentzian line shape fitted to the upper frequency half of the peak (dotted line). The asymmetry in the E_2^{high} line shape stems from the strong frequency dependence of the imaginary part of the phonon self-energy, which is plotted in Fig. 5 (dashed-dotted line) against the left axis over the frequency region where the E_2^{high} mode occurs. Such a strong variation of the imaginary part of the phonon self-energy in the vicinity of the E_2^{high} frequency has been previously shown to give rise to an anomalous behavior of the E_2^{high} linewidth in ZnO crystals with different isotopical compositions and to an unusual pressure dependence of the E_2^{high} linewidth vs hydrostatic pressure.[8] In the present work, we show that this self-energy features are also responsible for the line-shape asymmetry of the E_2^{high} Raman peak.

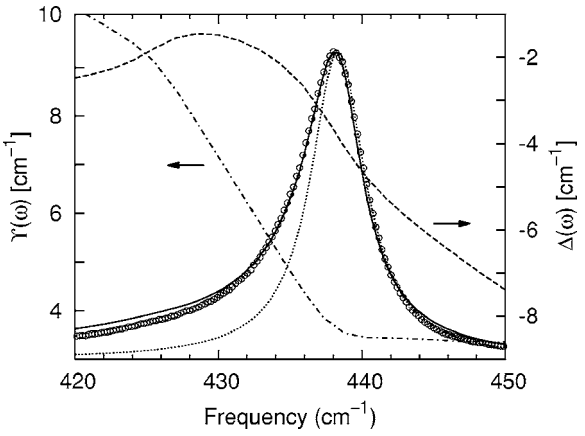

FIG. 5. High-resolution spectrum of the E_2^{high} mode of ZnO at room temperature (open circles). The solid line is the theoretical line shape calculated using the anharmonic decay model described in the text. For comparison, a symmetric Lorentzian line shape fitted to the high-frequency side of the peak is also displayed (dotted line). The real and imaginary parts of the phonon self-energy used in the calculations are plotted as dashed and dot-dashed lines, respectively.

The determination of the anharmonic coupling constants by fitting Eq. (7) to a single Raman spectrum has some degree of arbitrariness, as many combinations of $|V_3^+|^2$ and $|V_3^-|^2$ values yield similarly good visual agreement with the data. Instead of relying on a single Raman spectrum to derive the values of the anharmonic constants, we have measured the E_2^{high} linewidth for the full set of Raman spectra obtained at different temperatures and we have fitted the model to the temperature dependence of the E_2^{high} linewidth. To this end, the FWHM obtained from the theoretical line shape [Eq. (7)] Γ_{LS} was tabulated for a grid of $|V_3^+|^2$ and $|V_3^-|^2$ values. The tabulated values were used to interpolate $\Gamma_{\text{LS}}(T; |V_3^+|^2, |V_3^-|^2)$, which was fitted by the Levenberg-Marquardt method to the experimental linewidths. Including a constant background contribution to the linewidth (Γ_0) to account for defect and impurity scattering improves the fit significantly. The best fit to our data, which is displayed in Fig. 6, is obtained for $|V_3^+|^2 = 39$ cm^{-2}, $|V_3^-|^2 = 3.8$ cm^{-2}, and $\Gamma_0 = 1.3$ cm^{-1}. These results confirm that the decay rate for phonon-difference decay channels is considerably lower than for phonon-sum decay channels, and thus it can be safely neglected at low temperatures.

Estimates of the anharmonic squared matrix elements for the E_2^{high} mode of ZnO were obtained in Refs. 8 and 15 by using the expressions for the imaginary part of the self-energy [Eq. (4)] evaluated at the frequency of the mode and adjusting the anharmonic coefficients to reproduce their measured FWHM. As discussed above, when the frequency dependence is neglected, the imaginary part of the self-energy corresponds to the half width of the Lorentzian line shape, and therefore this procedure yields values for the anharmonic

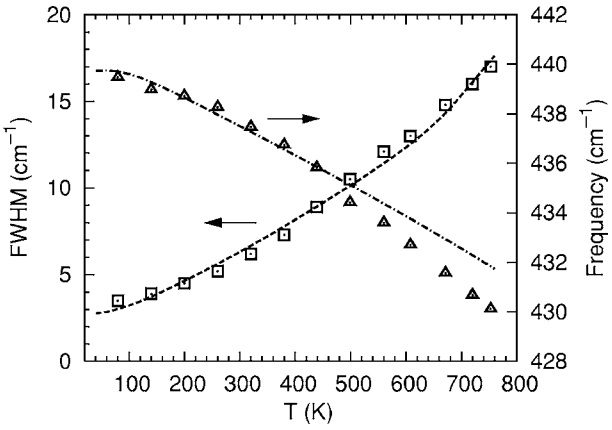

FIG. 6. Temperature dependence of the linewidth (squares, left axis) and frequency (triangles, right axis) of the E_2^{high} mode. The dashed line is a fit of the model discussed in the text to the linewidth data. The dot-dashed line corresponds to the temperature dependence of the frequency given by the model for the same set of parameters.

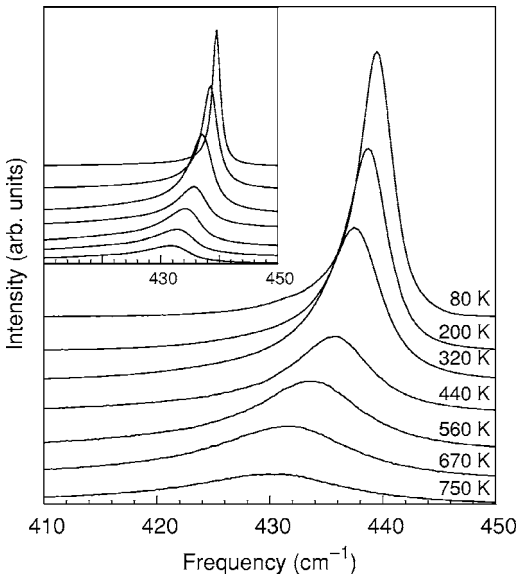

FIG. 7. Raman spectra of the E_2^{high} mode for temperatures in the 80–750 K range. Inset, corresponding line shapes calculated using the Fermi resonance model described in the text.

coefficients which are actually two times the values of the corresponding anharmonic squared matrix elements $[|V_3^+|^2$ and $|V_3^-|^2$ of Eq. (4)]. After correcting for this factor of 2, our values for the anharmonic squared matrix elements are somewhat higher than those given in Refs. 8 and 15 (39 vs 28 cm^{-1} for $|V_3^+|^2$ and 3.8 vs 3.1 cm^{-1} for $|V_3^-|^2$). In those works, no defect and/or impurity contribution to the linewidth was considered. If we do not include the constant contribution Γ_0 in our fits, the resulting $|V_3^-|^2$ value increases appreciably to compensate for the defect and/or impurity broadening, while $|V_3^+|^2$ turns out to be roughly the same. This explains the value $|V_3^-|^2$=5.8 cm^{-2} used to obtain the visual fit displayed in Fig. 5, but cannot account for the lower $|V_3^-|^2$ value reported in Ref. 8. The discrepancies in the $|V_3^+|^2$ and $|V_3^-|^2$ values mentioned above could arise from the simplified model used in Refs. 8 and 15, which does not take into account the actual frequency dependence of the phonon self-energy. Also, one should bear in mind that the higher-order terms neglected in Eq. (3) may lead to deviations in the calculated line shapes that are of increasing importance for higher temperatures. This could explain that the measured E_2^{high} frequency falls slightly below the one calculated from the model for $T>500$ K using the parameters determined above (see Fig. 6).[29]

Figure 7 displays high-resolution E_2^{high} spectra recorded at temperatures in the 80–750 K range. As temperature increases, the E_2^{high} peak is reduced in intensity and broadens significantly, maintaining a visible asymmetry toward lower frequencies. Such behavior is well reproduced by the line shapes calculated according to Eq. (7), which are plotted in the inset of Fig. 7. Note that Eq. (7) does not contain the defect and/or impurity broadening contribution and consequently the calculated line shapes are narrower than the corresponding Raman spectra, which are further broadened by defects and impurities. This is most apparent for the narrowest Raman line shape measured at 80 K.

2. The $A_1(LO)$ and $E_1(LO)$ modes: Generalized Ridley channel model

The A_1(LO) and E_1(LO) frequencies of ZnO are very close to each other. Unlike the E_2^{high} mode, these two modes occur at frequencies that lie in a plateau of the two-phonon DOS with a relatively high density of states. Therefore their line shape is not affected by variations of the phonon self-energy and a simpler model can be used to analyze their temperature dependence. Inspection of the phonon dispersion curves[15] suggests that the main decay channel for these modes is the so-called generalized Ridley channel.[30,31] This involves the decay of the longitudinal optical mode into a mode of the transverse acoustic branches and a mode of the transverse optical branches. The anisotropy of the force constants in the wurtzite structure causes the transverse branches to split along the main symmetry lines of the Brillouin zone. Thus, modes from different split TO and TA branches can provide decay channels for both the A_1(LO) and the E_1(LO) modes. In the TA region, the phonon DOS presents a maximum at 100 cm^{-1}, with a significant contribution from the lower TA branch along *L*-*M*. A secondary maximum can be seen at ≈120 cm^{-1}, with an important contribution from the nearly flat TA branch along *L*-*M*. Similarly, in the TO region the phonon DOS exhibits a maximum at ≈455 cm^{-1} and a secondary maximum at ≈490 cm^{-1}, both of which contain important contributions from the split TO branches along *L*-*M*. Taking into account the phonon DOS, the A_1(LO) mode (574 cm^{-1}) decays most probably into pairs of TO and TA modes with frequencies around 455 and 120 cm^{-1}, respectively, whereas the corresponding decay frequencies for the E_1(LO) mode (590 cm^{-1}) are clustered around 490 and 100 cm^{-1}.

Assuming that the most relevant decay channel is the generalized Ridley channel with the main contributions clustered around ω_1 and ω_2, the temperature-dependent FWHM of the phonon mode can be modeled by[28]

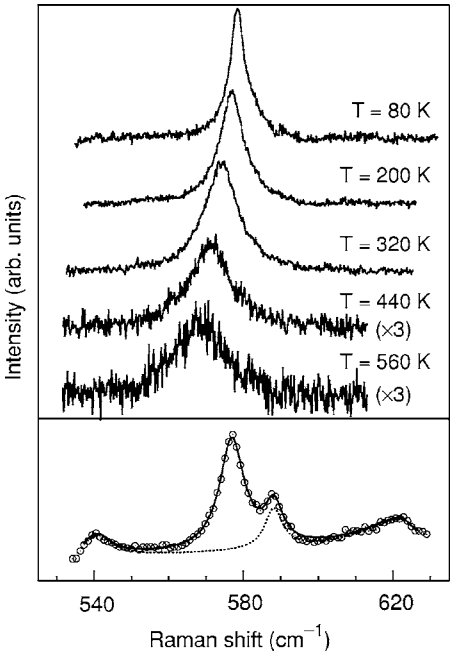

FIG. 8. Raman spectra of the A_1(LO) mode for temperatures in the 80–560 K temperature range, after baseline subtraction. For $T \geq 440$ K the spectra were recorded with the microscope hot stage and therefore the signal is lower due to the smaller depth of focus of the setup. Lower panel, fit to the Raman data (circles) used to determine the baseline (dotted line) to be subtracted, for the spectrum at $T=200$ K, where an additional peak is already resolved.

$$\Gamma(T) = \Gamma_0 + A[1 + n(\omega_1, T) + n(\omega_2, T)], \tag{8}$$

where Γ_0 is a background contribution due to impurity and/or defect scattering and isotopic broadening, A is the anharmonic coefficient, and $n(\omega, T)$ is the Bose-Einstein distribution function. Similarly, the temperature dependence of the frequency of the phonon mode can be written as

$$\omega(T) = \omega_0 + \Delta_0(T) + B[1 + n(\omega_1, T) + n(\omega_2, T)], \tag{9}$$

where $\Delta_0(T)$ is the thermal expansion shift given by Eq. (6) and B is the anharmonic coefficient.

As can be seen in Figs. 2 and 3, the A_1(LO) mode is very weak and emerges on a relatively strong second-order Raman scattering background. Furthermore, at low temperatures a peak at slightly higher frequency is resolved. To perform a linewidth analysis of the A_1(LO) Raman peak both contributions must be subtracted from the spectra. In Fig. 8 we show $z(xx)\bar{z}$ Raman spectra of the A_1(LO) mode for temperatures in the 80–560 K range after background subtraction. To determine the spectra backgrounds, a suitable combination of Lorentzian line shapes plus a linear background were fitted to the spectra, as illustrated in the lower panel of Fig. 8 for the spectrum at 200 K. The A_1(LO) Raman peak exhibits a symmetrical Lorentzian line shape, which redshifts and broadens as temperature increases. For $T \geq 400$ K the microscope hot stage was used, and hence the signal level is lower because of the smaller depth of focus of the setup.

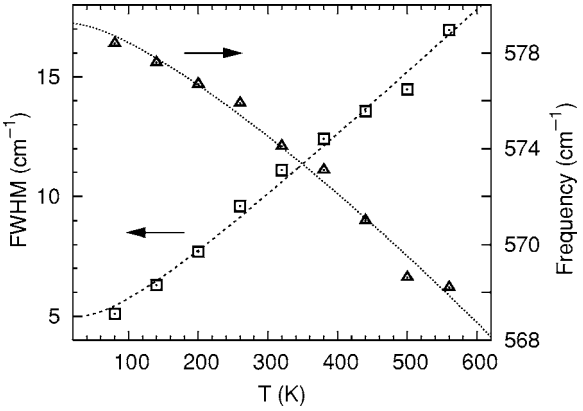

FIG. 9. Measured values of frequency (triangles) and linewidth (squares) of the A_1(LO) mode for temperatures in the 80–560 K range. The dotted lines are fits of $\Gamma(T)$ and $\omega(T)$ given by Eqs. (8) and (9) to the respective data.

Measurements at $T > 560$ K were discarded as the signal-to-noise ratio did not allow a reliable determination of the peak width.

The measured Raman shifts and linewidths of the A_1(LO) mode are plotted in Fig. 9. Equations (8) and (9), with $\omega_1 = 120$ cm^{-1} and $\omega_2 = 455$ cm^{-1}, and Γ_0, A, ω_0, and B as adjustable parameters, were fitted to the respective experimental data. We find $\Gamma_0 = 1.3$ cm^{-1}, $A = 3.7$ cm^{-1}, $\omega_0 = 581.4$ cm^{-1}, and $B = -2.1$ cm^{-1}.

A similar analysis was performed for the E_1(LO) mode. Figure 10 displays the $x(zy)y$ Raman spectra of the E_1(LO) mode for temperatures between 80 and 380 K, after careful subtraction of the background as illustrated in the lower panel for the 320 K spectrum. Since the E_1(LO) mode is

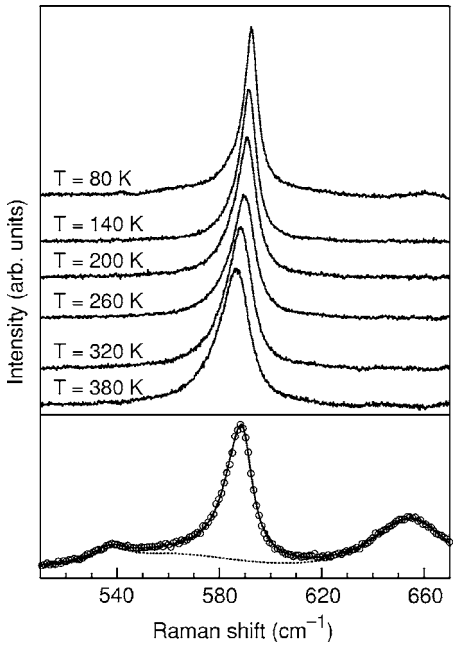

FIG. 10. Raman spectra of the E_1(LO) mode for temperatures in the 80–380 K temperature range, after baseline subtraction. Lower panel, fit to the Raman data (circles) used to determine the baseline (dotted line) to be subtracted, for the spectrum at $T=320$ K.

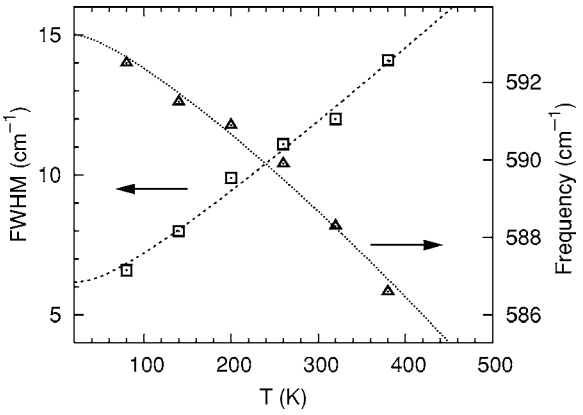

FIG. 11. Measured values of frequency (triangles) and linewidth (squares) of the E_1(LO) mode for temperatures in the 80–380 K range. The dotted lines are fits of $\Gamma(T)$ and $\omega(T)$ given by Eqs. (8) and (9) to the respective data.

forbidden in backscattering configuration, the microscope hot stage could not be used and consequently this set of measurements was only possible on a limited temperature range. Measured E_1(LO) linewidths and frequencies as well as linear-square fits of Eqs. (8) and (9) to the data with $\omega_1 = 100$ cm^{-1} and $\omega_2 = 490$ cm^{-1} are plotted in Fig. 11. The best fit to our data is found for $\Gamma_0 = 2.8$ cm^{-1}, $A = 3.3$ cm^{-1}, $\omega_0 = 595$ cm^{-1}, and $B = -1.7$ cm^{-1}.

By comparing the anharmonic coefficients A and B for the A_1(LO) and E_1(LO) modes of ZnO we can see that the temperature dependence of these modes is very similar. This is not unexpected, as these modes lie close in frequency in a region where the two-phonon DOS does not change appreciably. However, the E_1(LO) mode displays a larger linewidth, which implies a higher value of Γ_0 and suggests that the E_1(LO) mode is more strongly affected by impurity and/or defect scattering than the A_1(LO) mode. As the incorporation of defects in ZnO is known to be highly anisotropic, this could be related to a possible anisotropy in the distribution of defects and the fact that the E_1(LO) mode has an in-plane atomic motion whereas the atomic motion of the A_1(LO) mode takes place along the c axis.

To sum up, in contrast with the E_2^{high} mode where anharmonic decay involves a continuum of TA+LA phonons, the temperature dependence of the A_1(LO) and E_1(LO) modes can be accounted for by a simple model in which the longitudinal phonon decays into a pair of TO and TA phonons whose frequencies correspond to maxima of the phonon DOS.

3. Phonon lifetimes

The phonon lifetime τ can be derived from the Raman spectra via the energy-time uncertainty relation

$$\frac{1}{\tau} = \frac{\Delta E}{\hbar} = 2\pi c\Gamma, \tag{10}$$

where ΔE is the uncertainty in the energy of the phonon mode, $\hbar$ is the Planck constant, and Γ is the FWHM of the Raman peak in units of cm^{-1}.

TABLE III. Phonon lifetimes of the E_2^{high}, A_1(LO), and E_1(LO) modes of ZnO at 80 K and room temperature. The characteristic decay time associated with impurities τ_I is estimated from the background broadening parameter Γ_0 used to fit the FWHM temperature dependence.

	$T=80$ K		$T=300$ K			
Phonon mode	Γ (cm^{-1})	τ (10^{-12} s)	Γ (cm^{-1})	τ (10^{-12} s)	Γ_0 (cm^{-1})	τ_I (10^{-12} s)
E_2^{high}	3.5	1.5	6.0	0.88	1.3	4.1
A_1(LO)	5.1	1.0	9.7	0.54	1.3	4.1
E_1(LO)	6.6	0.80	11.7	0.45	2.8	1.9

Phonon lifetime is mainly limited by two mechanisms: (i) anharmonic decay of the phonon into two or more phonons so that energy and momentum are conserved, with a characteristic decay time τ_A and (ii) perturbation of the translational symmetry of the crystal by the presence of impurities, defects and isotopic fluctuations, with a characteristic decay time τ_I. The phonon lifetime deduced from the Raman measurements is therefore

$$\frac{1}{\tau} = \frac{1}{\tau_A} + \frac{1}{\tau_I}. \tag{11}$$

It is difficult to separate the contribution of both mechanisms, but we can obtain an estimation of the characteristic decay time associated with impurities from the values of the Γ_0 parameter provided by the FWHM temperature-dependence fits. The results are summarized in Table III. We can see that the shortest τ_I corresponds to the E_1(LO) mode. The fact that the E_1(LO) mode has a polar character allows a Fröhlich interaction with charged impurities and defects.[32] As already discussed, owing to a possible anisotropy in the distribution of defects such interaction could affect the E_1(LO) lifetime more severely than the A_1(LO) lifetime, as the E_1(LO) mode has in-plane polarization, whereas the A_1(LO) mode is polarized along the c axis. This would explain that the E_1(LO) linewidth observed both at 80 K and at RT is 1.5–2 cm^{-1} higher than the corresponding A_1(LO) linewidth.

The E_2^{high} lifetime at room temperature is in good agreement with the value reported by Bergman *et al.*[9] No values for the A_1(LO) and E_1(LO) were reported in that work. We find similar lifetime values around 0.5 ps for both modes, which are close to those reported for high-quality AlN crystals.[9] The values found for the E_2^{high}, A_1(LO), and E_1(LO) phonon lifetimes corroborate that the anharmonic decay involves in all three cases a three-phonon process and rules out four-phonon interaction as the main decay mechanism, as this would yield phonon lifetimes 2 or 3 orders of magnitude longer.

IV. SUMMARY AND CONCLUSIONS

We have carried out a detailed study of the first- and second-order Raman scattering of ZnO for temperatures

ranging from 80 up to 750 K. Second-order Raman spectra obtained in different scattering geometries have been discussed in terms of DFT phonon dispersion relations and symmetry analysis. Characteristic second-order Raman peaks have been assigned to overtones and combinations of acoustic and optical phonon branches. The temperature dependence of the 333 cm^{-1} Raman peak, which is often attributed to acoustic overtones at M, has been shown to correspond to a difference mode, and the mode has been assigned to E_2^{high}-E_2^{low}. Several sharp peaks show up at low temperature, which are tentatively related to intrinsic lattice defects. Most notably, a peak is resolved at 589 cm^{-1} in the $z(xx)\bar{z}$ spectra at 80 K, very close to the E_1(LO) frequency. The possibility of a leaky E_1(LO) mode can be ruled out since the frequency of the E_1(LO) mode at 80 K was determined to be 593 cm^{-1} in the allowed $x(zy)y$ configuration.

The anharmonic broadening of the E_2^{high}, A_1(LO), and E_1(LO) phonon modes was studied as a function of temperature. The E_2^{high} mode of ZnO exhibits a visibly asymmetric line shape, which could be successfully explained in terms of resonant anharmonic interaction of the E_2^{high} mode with a band of combined transverse and longitudinal acoustic modes, as the steep variation of the two-phonon DOS around the E_2^{high} frequency leads to a distorted phonon line shape. In contrast, the two-phonon DOS is rather flat in the A_1(LO) and E_1(LO) frequency region and the temperature dependence of these modes can be adequately described with a simple anharmonic decay model via a dominating Ridley channel involving TO and TA modes whose frequencies are clustered around maxima of the DOS. The lifetimes of these modes are determined from the Raman spectra and are found to be around 0.5 ps for both longitudinal modes at room temperature.

ACKNOWLEDGMENTS

This work has been supported by the Spanish Ministry of Education and Science under Contract No. MAT2004-0664 and Ramón y Cajal Program. The work performed by the United States Air Force Research Laboratory at Hanscom Air Force Base was partially supported by the Air Force Office of Scientific Research.

[1] D. C. Look, Mater. Sci. Eng., B **80**, 383 (2001).
[2] B. C. Lee, K. W. Kim, M. A. Stroscio, and M. Dutta, Phys. Rev. B **58**, 4860 (1998).
[3] N. Hasuike, H. Fukumura, H. Harima, K. Kisoda, H. Matsui, H. Saeki, and H. Tabata, J. Phys.: Condens. Matter **16**, S5807 (2004).
[4] W. Limmer, W. Ritter, R. Sauer, B. Mensching, C. Liu, and B. Rauschenbach, Appl. Phys. Lett. **72**, 2589 (1998).
[5] D. Pastor, R. Cuscó, L. Artús, G. González-Díaz, S. Fernández, and E. Calleja, Semicond. Sci. Technol. **20**, 374 (2005).
[6] A. Göbel, T. Ruf, C.-T. Lin, M. Cardona, J.-C. Merle, and M. Joucla, Phys. Rev. B **56**, 210 (1997).
[7] J. M. Zhang, T. Ruf, M. Cardona, O. Ambacher, M. Stutzmann, J.-M. Wagner, and F. Bechstedt, Phys. Rev. B **56**, 14399 (1997).
[8] J. Serrano, F. J. Manjón, A. H. Romero, F. Widulle, R. Lauck, and M. Cardona, Phys. Rev. Lett. **90**, 055510 (2003).
[9] L. Bergman, D. Alexson, P. L. Murphy, R. J. Nemanich, M. Dutta, M. A. Stroscio, C. Balkas, H. Shin, and R. F. Davis, Phys. Rev. B **59**, 12977 (1999).
[10] A. Link, K. Bitzer, W. Limmer, R.Sauer, C. Kirchner, V. Schwegler, M. Kamp, D. G. Ebling, and K. W. Benz, J. Appl. Phys. **86**, 6256 (1999).
[11] T. C. Damen, S. P. S. Porto, and B. Tell, Phys. Rev. **142**, 570 (1966).
[12] C. A. Arguello, D. L. Rosseau, and S. P. S. Porto, Phys. Rev. **181**, 1351 (1969).
[13] J. M. Calleja and M. Cardona, Phys. Rev. B **16**, 3753 (1977).
[14] D. G. Mead and G. R. Wilkinson, J. Raman Spectrosc. **6**, 123 (1977).
[15] J. Serrano, A. H. Romero, F. J. Manjón, R. Lauck, M. Cardona, and A. Rubio, Phys. Rev. B **69**, 094306 (2004).
[16] C. Aku-Leh, J. Zhao, R. Merlin, J. Menéndez, and M. Cardona, Phys. Rev. B **71**, 205211 (2005).
[17] M. Suscavage *et al.*, MRS Internet J. Nitride Semicond. Res. **4S1**, G3.40 (1999).
[18] H. Siegle, G. Kaczmarczyk, L. Filippidis, A. P. Litvinchuk, A. Hoffmann, and C. Thomsen, Phys. Rev. B **55**, 7000 (1997).
[19] A. Kaschner, U. Haboeck, M. Strassburg, G. Kaczmarczyk, A. Hoffmann, C. Thomsen, A. Zeuner, H. R. Alves, D. M. Hofmann, and B. K. Meyer, Appl. Phys. Lett. **80**, 1909 (2002).
[20] *Light Scattering in Solids II*, edited by M. Cardona and G. Güntherodt, Topics in Applied Physics Vol. 50 (Springer-Verlag, Berlin, 1982).
[21] C. Bundesmann, N. Ashkenov, M. Shubert, D. Spemann, T. Butz, E. M. Kaidashev, M. Lorenz, and M. Grundmann, Appl. Phys. Lett. **83**, 1974 (2003).
[22] B. A. Weinstein, Solid State Commun. **20**, 999 (1976).
[23] F. Widulle, T. Ruf, A. Göbel, E. Schönherr, and M. Cardona, Phys. Rev. Lett. **82**, 5281 (1999).
[24] R. A. Cowley, Rep. Prog. Phys. **31**, 123 (1968).
[25] W. J. Borer, S. S. Mitra, and K. V. Namjoshi, Solid State Commun. **9**, 1377 (1971).
[26] H. Iwanaga, A. Kunishige, and S. Takeuchi, J. Mater. Sci. **35**, 2451 (2000).
[27] A. Debernardi and M. Cardona, Phys. Rev. B **54**, 11305 (1996).
[28] J. Menéndez and M. Cardona, Phys. Rev. B **29**, 2051 (1984).
[29] A. Debernardi and M. Cardona, Physica B **263-264**, 687 (1999).
[30] B. K. Ridley, J. Phys.: Condens. Matter **8**, L511 (1996).
[31] S. Barman and G. P. Srivastava, Phys. Rev. B **69**, 235208 (2004).
[32] B. K. Ridley and R. Gupta, Phys. Rev. B **43**, 4939 (1991).